Two-dimensional electron gas density in $Al_{1-x}In_xN/AlN/GaN$ heterostructures ($0.03 \leq x \leq 0.23$)

M. Gonschorek,[1,a] J.-F. Carlin,[1] E. Feltin,[1] M. A. Py,[1] N. Grandjean,[1] V. Darakchieva,[2] B. Monemar,[2] M. Lorenz,[3] and G. Ramm[3]
[1]*Institute of Quantum Electronics and Photonics, Ecole Polytechnique Fédérale de Lausanne (EPFL), CH-1015 Lausanne, Switzerland*
[2]*Department of Physics, Chemistry and Biology, Linköping University, S-581 83 Linköping, Sweden*
[3]*Institut für Experimentelle Physik II, Fakultät für Physik und Geowissenschaften, Universität Leipzig, Linnéstraße 3-5, 04103 Leipzig, Germany*

(Received 23 January 2008; accepted 2 March 2008; published online 12 May 2008)

Compared to the AlGaN alloy, which can only be grown under tensile strain on GaN, the AlInN alloy is predicted by Vegard's law to be lattice-matched (LM) on fully relaxed GaN templates for an indium content of ~17.5%, i.e., it can be grown either tensely or compressively on GaN. The effect of strain on the polarization induced sheet charge density at the $Al_{1-x}In_xN/AlN/GaN$ heterointerfaces is carefully investigated for 6 and 14 nm thick AlInN barriers including a 1 nm thick AlN interlayer. The barrier indium content ranges at $0.03 \leq x \leq 0.23$ for 6 nm thick barriers and $0.07 \leq x \leq 0.21$ for 14 nm thick barriers. It is found that the two-dimensional electron gas (2DEG) density varies between $(3.5 \pm 0.1) \times 10^{13}$ cm^{-2} and $(2.2 \pm 0.1) \times 10^{13}$ cm^{-2} for 14 nm thick barriers. Finally, a 2DEG density up to $(1.7 \pm 0.1) \times 10^{13}$ cm^{-2} is obtained for a nearly LM AlInN barrier with ~14.5% indium on GaN as thin as 6 nm. © *2008 American Institute of Physics*.
[DOI: 10.1063/1.2917290]

I. INTRODUCTION

Nowadays, state-of-the-art $Al_xGa_{1-x}N/GaN$ high electron mobility transistors (HEMTs) grown on SiC substrates with a barrier Al composition of 40% exhibit maximum drain-source current densities of ~1.5 A/mm.[1] The limitation arises from the tensile strain that builds up in the AlGaN barrier and eventually leads to plastic relaxation above a critical thickness for large Al contents. A promising approach to overcome this limit is the growth of high quality nearly lattice-matched (LM) AlInN/GaN heterostructures.[2] Indeed, one of the main features of these LM heterostructures is the possibility to keep a high polarization induced sheet charge density at the heterointerface even for a vanishing piezoelectric component due to the absence of strain. Actually, a net positive charge appears at the interface because of the difference in spontaneous polarization between AlInN and GaN.[3] Then, electrons from surface states and residual donors tend to compensate for these polarization charges forming a two-dimensional electron gas (2DEG) whose density is of the order of 2.6×10^{13} cm^{-2}.[4] This gives rise to high performance HEMTs grown on *c*-plane sapphire substrates with above 2 A/mm drain-source current densities and a cutoff frequency of 26 GHz.[5] Similar heterostructures grown on SiC substrates exhibit an output power of up to 6.8 W/mm at 10 GHz.[6] This demonstrates the strong potential of this system, whereas only scarce information is available on the amount of piezoelectric and pyroelectric charges as a function of the In composition, the influence of the AlInN barrier thickness, and more generally, on the values of lattice constants, their bowing parameters, and the strain state of the underlying GaN buffer layer.

In this paper, we report on a detailed study of the 2DEG density in $Al_{1-x}In_xN/AlN/GaN$ heterostructures with $0.03 \leq x \leq 0.23$. The effects of both In composition and barrier thickness are investigated.

II. GROWTH AND EXPERIMENTS

Epilayers are grown in an AIXTRON 200/4 RF-S metal organic vapor phase epitaxy (MOVPE) system on 2 in. *c*-plane sapphire substrates. The growth is initiated by a low-temperature (LT) GaN nucleation layer followed by a 2 μm thick undoped GaN buffer layer, using trimethylgallium, nitrogen and hydrogen as carrier gases. The buffer layer was checked to exhibit a net residual doping density $(N_D - N_A)$ below 10^{14} cm^{-3} to reduce the parasitic conduction paths as much as possible . The samples were then cooled down to grow the AlInN layers by using growth conditions previously optimized for LM AlInN heterostructures, while the indium content was altered by varying the temperature during the growth.[7,8] A thin ~1 nm AlN interlayer was inserted in all samples to achieve a larger separation of the electron wave function from the AlInN barrier to decrease the impact of interface roughness and alloy scattering. This results in an improvement of the lateral transport properties of the 2DEG.[4] Secondary neutral mass spectroscopy (SNMS) is employed for a qualitative layer composition analysis. Reciprocal space maps (RSMs) are recorded with a high resolution x-ray diffractometer (HRXRD) using Cu $K\alpha_1$ radiation ($\lambda = 1.540\,562$ Å). The 2DEG density (n_s) is measured using temperature-dependent standard Van der Pauw–Hall

[a]Electronic mail: marcus.gonschorek@epfl.ch.

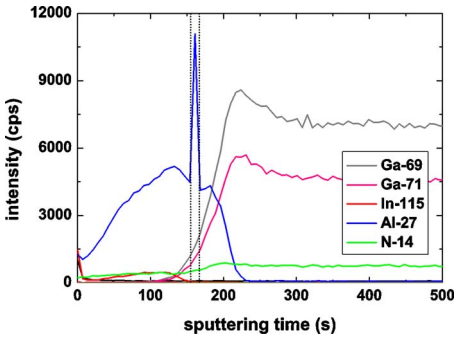

FIG. 1. (Color online) SNMS sputtering profile: The 0–160 s range corresponds to the $Al_{0.855}In_{0.145}N$ barrier, the 160–170 s range corresponds to the AlN interlayer (sharp peak in the detected Al composition), while the GaN buffer layer corresponds to sputtering times exceeding 170 s. Dotted lines are a guide for the eyes and mark the position of the AlN interlayer.

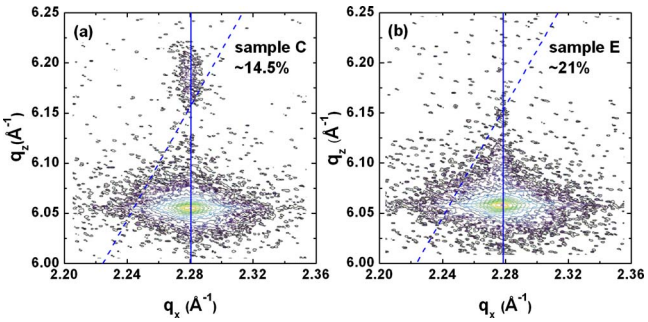

FIG. 2. (Color online) (105) reciprocal space maps for 14 nm thick AlInN layers deposited on GaN. (a) and (b) correspond to samples C and E, respectively. AlInN layers with indium contents below 16.5% (sample C) are pseudomorphic to GaN, while for layers with larger indium contents an onset of relaxation is observed (sample E). Fully relaxed and pseudomorphic growth is given by dashed and full lines, respectively.

and low-frequency electrochemical capacitance voltage (*C-V*) techniques. The photoluminescence (PL) was carried out under weak excitation power density using the 244 nm line of a continuous wave Ar^+ laser frequency doubling unit at 8 K.

III. RESULTS AND DISCUSSION

A. Structural properties

Figure 1 shows a SNMS sputtering profile of an $Al_{0.855}In_{0.145}N/AlN$ (1 nm)/GaN/sapphire sample with ~13 nm barrier thickness. The AlN interlayer manifests itself as a sharp peak in the Al concentration profile for sputtering times between 160 and 170 s. The detected intensities of Ga, Al, and In species between 0 and 160 s sputtering times confirm that the barrier only consists of the AlInN alloy. Notice that SNMS is not a suitable method to measure the stoichiometry of thin films, since a reference sample is needed with an *a priori* well-defined composition to determine the sensitivity factors. In addition, the exponential decay of the intensities does not allow drawing of conclusions on diffusion or concentration gradients since they even appear for layers with constant homogeneous compositions and are hence inherent to this method.[9] However, we can firmly state from SNMS analysis that there is no or at least only a minor Ga diffusion into the AlInN barrier.

Recently, Lorenz *et al.*[10] clarified the deviation observed between the indium compositions determined by HRXRD analysis from the actual indium composition obtained by nondestructive Rutherford backscattering (RBS) using nonzero lattice constant bowing parameters equal to −0.010 Å and −0.075 Å for the *a* and *c* lattice constants, respectively. This led to the LM condition for AlInN on fully relaxed GaN corresponding to an indium composition of 17.1%. To determine the *c* lattice constants of GaN and AlInN layers, symmetric (002) scans have been performed. Then, the lattice parameter *c* is directly given by the Bragg relation $c = l \cdot \lambda / (2 \sin \Theta_B)$, where *l* is the Miller index in (*hkl*) notation and Θ_B is the Bragg angle.[11] Alternatively, *a* and *c* can be read out from the RSM for an asymmetric reflection by using the relations $a = 2\pi / q_x \cdot \sqrt{4/3(h^2+k^2+hk)}$ and $c = 2\pi / q_z \cdot l$, with q_x and q_z the lateral and transverse scattering vectors, respectively. Note that a slight error can be introduced because for asymmetric reflections, the intensity maximum does not appear at the Bragg angle.[12] Figure 2 shows RSMs for the (105) reflection for a sample with the AlInN barrier under tensile strain (sample C) and under compressive strain (sample E). Information on the residual strain of the GaN buffer layer can confidently be determined from the LT PL of the GaN bandedge.[13,14] The free exciton (FX_A) energy (Table I) indicates that the GaN buffer layer is under a slight in-plane compressive strain $\varepsilon_{\parallel} = (a - a_0)/a_0$, where a_0 is the relaxed parameter of GaN, which varies between −0.11% and −0.19% for the different samples (relaxed GaN lattice parameters are assumed to be $a = 3.1876$ Å and $c = 5.1846$ Å).[12] The observed differences in residual strain for the GaN buffer layer of the various samples might be

TABLE I. Main structural parameters of samples with increasing indium content with 14 nm thick AlInN barriers: LT GaN FX_A energy, GaN lattice constants, AlInN lattice constants, and indium composition deduced from Vegard's law and by using the bowing parameters $b_a = -0.010$ Å and $b_c = -0.075$ Å given in Ref. 10 and RBS indium content.

Sample	FX_A energy (eV)	a_{GaN} (Å)	c_{GaN} (Å)	a_{AlInN} (Å)	c_{AlInN} (Å)	Indium content (Vegard's law) (%)	Indium content for $b_a = -0.010$ Å $b_c = -0.075$ Å (%)	Indium content RBS (%)
A	3.4895	3.1821	5.1892	3.1821	5.0008	7.8	7.2	7
B	3.4896	3.1821	5.1892	3.1821	5.0588	13.1	12.2	12
C	3.4906	3.1817	5.1895	3.1817	5.0835	15.3	14.3	14.5
D	3.4865	3.1831	5.1883	3.1839	5.1369	19.8	18.7	19.5
E	3.4835	3.1842	5.1875	3.1863	5.1615	21.8	20.6	21

attributed to a slight change in their respective growth conditions. Then, the reciprocal lattice vectors at the maximum intensity of the GaN reflection in the RSM were corrected to the lattice parameters obtained from GaN bandedge luminescence from which the lattice parameters of the AlInN barriers were deduced.

Results are summarized in Table I. The alloy concentration for strained layers is usually assigned by employing the relaxed lattice constants for the alloy and by assuming the validity of the elastic continuum theory, i.e., which the relation for conventional biaxial strain holds. If one relies on the bowing parameters given in Ref. 10 one obtains an indium composition range between 7.2% and 20.6%. The actual indium content for the lattice matching condition also depends on the strain state of the underlying GaN layer. In the case of a completely relaxed GaN layer with $a=3.1876$ Å, it should be met at 17.1%. For a slight compressive strain, as it is the case for our samples with $a=3.1825$ Å, it occurs at 16.5%. In addition, RBS was also performed to determine the indium content of these layers with an accuracy of $\pm 0.5\%$ and to show, overall, a good agreement with XRD values.[15] Further, we have found that samples grown in the compressive strain regime ($x>16.5\%$) exhibit slight relaxations of $\sim 5\%$ and $\sim 10\%$ for samples D and E, respectively. Since the intensity of the AlInN peak in RSMs is slightly shifted to lower scattering vectors, this corresponds to an a_{AlInN}, which is slightly larger than a_{GaN}. Note that relaxation mechanisms have been reported for 100 nm unannealed AlInN films where partial relaxation was observed for In content deviations of $\pm 3\%$ from the LM composition, regardless whether layers were compressively or tensely strained.[16] For ~ 120 nm thick compressively grown $Al_{0.76}In_{0.24}N$ layers, the relaxation is accompanied by the formation of two distinct sublayers of different In compositions.[15,17] Note that for thin layers, it is difficult to determine the actual origin of this relaxation. The latter might be related to an onset of phase separation or a composition depth gradient.

B. Electrical properties

Let us now describe the electronic properties of those heterostructures. An interface charge builds up due to the abrupt change of the polarization per volume across the AlInN/GaN heterointerface.[3,18] The total polarization charge density is the sum of spontaneous polarization (P_{sp}) and piezoelectric polarization (P_{pz}), which gives an upper limit for the 2DEG density formed at the heterointerface. Free electrons compensate the positive polarization charges, forming a 2DEG at the heterointerface, whose density can be described by the following implicit equation:[18]

$$n_s(x) = \frac{\sigma(x)}{e} - \left[\frac{\varepsilon_0 \varepsilon(x)}{d_{\mathrm{AlInN}} e^2}\right]\{e\Phi_b(x) + E_F[x, n_s(x)] - \Delta E_C(x)\}, \tag{1}$$

where σ is the total bound sheet charge density, e is the electron charge, ε and ε_0 are the relative dielectric constant and the dielectric permittivity of the vacuum, respectively, d_{AlInN} is the thickness of the barrier, $e\Phi_b$ is the Schottky barrier height, E_F is the Fermi level with respect to the GaN conduction band, and ΔE_C is the conduction band offset between AlInN and GaN, which depends on the In composition x. In the limit of large barrier thicknesses, the 2DEG density approaches the total bound sheet density $\sigma(x)/e$. Since we are dealing with AlInN/AlN/GaN heterostructures, the effect of the AlN interlayer can be taken into account by using an effective band offset $\Delta E_{C,\mathrm{eff}}$, corresponding to the energy difference of the AlInN and GaN conduction bands on both sides of the AlN interlayer.[19] The potential drop across the AlN interlayer can be approximated by[18]

$$\Delta E_{C,\mathrm{AlN}} = \frac{e^2}{\varepsilon_0 \varepsilon}\left(\frac{\sigma_{\mathrm{AlN}}}{e} - n_s\right) \Big/ d_{\mathrm{AlN}}, \tag{2}$$

where σ_{AlN} is the total polarization charge across an AlN/GaN interface and d_{AlN} is the AlN interlayer thickness. Thus, the effective band offset is given by

$$\Delta E_{C,\mathrm{eff}} = \Delta E_{C,\mathrm{AlN/GaN}} - \Delta E_{C,\mathrm{AlInN/AlN}} + \Delta E_{C,\mathrm{AlN}}, \tag{3}$$

where $\Delta E_{C,\mathrm{AlN/GaN}}$ is the band offset at the AlN/GaN heterointerface and $\Delta E_{C,\mathrm{AlInN/AlN}}$ is the band offset at the AlInN/AlN heterointerface. In contrast to the experimentally measured band offset at the AlN/GaN heterointerface of ~ 1.42 eV,[20] there is only scarce experimental values for the AlInN/AlN band offset. Thus, we rely on the relation $\Delta E_{C,\mathrm{ABN}} = 0.63\,[E_{g,\mathrm{ABN}}(x) - E_{g,\mathrm{ABN}}(0)]$ and a band gap bowing parameter of ~ 5 eV for the AlInN alloy.[21] Inserting Eq. (3) in Eq. (1) and neglecting the n_s dependence of Eq. (2) yield

$$n_s = \frac{1}{(d_{\mathrm{AlInN}} + d_{\mathrm{AlN}})} \times \left\{ \frac{\sigma_{\mathrm{AlInN}} \cdot d_{\mathrm{AlInN}}}{e} + \frac{\sigma_{\mathrm{AlN}} \cdot d_{\mathrm{AlN}}}{e} - \frac{\varepsilon_0 \varepsilon(x)}{e^2} \times \{e\Phi_b(x) + E_F[x, n_s(x)] - \Delta E_{C,\mathrm{AlN/GaN}} + \Delta E_{C,\mathrm{AlInN/AlN}}(x)\} \right\}. \tag{4}$$

From Eq. (4) the role of the interlayer becomes obvious. If the thickness of the AlN interlayer is thicker than the critical thickness to form a 2DEG, the AlN layer will be the main contributor. However, if the AlN interlayer is thinner than this critical thickness, the AlInN layer on top of it will be the main contributor to the 2DEG density. An AlN interlayer of ~ 1 nm confidently lies below the critical thickness to form a 2DEG.[8,22] On the other hand, the sum of negative polarization charges at the AlInN/AlN interface and positive polarization charges at the AlN/GaN interface equals the polarization charges of the AlInN/GaN heterostructure without an interlayer. Thus, an extrapolation of the bound sheet charges via AlInN barrier thickness variation using Eq. (4) will give the difference in polarization charges corresponding to the single heterostructure. Furthermore, an increase in the AlN interlayer thickness from 0 to 2 nm will also slightly increase the 2DEG density by an amount of $\sim 0.4 \times 10^{13}$ cm^{-2}. Similar effects of an AlN interlayer are also reported for AlGaN/AlN/GaN heterostructures.[23] Figure 3 shows a self-consistent band structure calculation[24] for an $Al_{0.855}In_{0.145}N/AlN/GaN$ heterostructure with 0, 1, and 2 nm thick AlN interlayers. The inset shows the calculated and measured 2DEG density

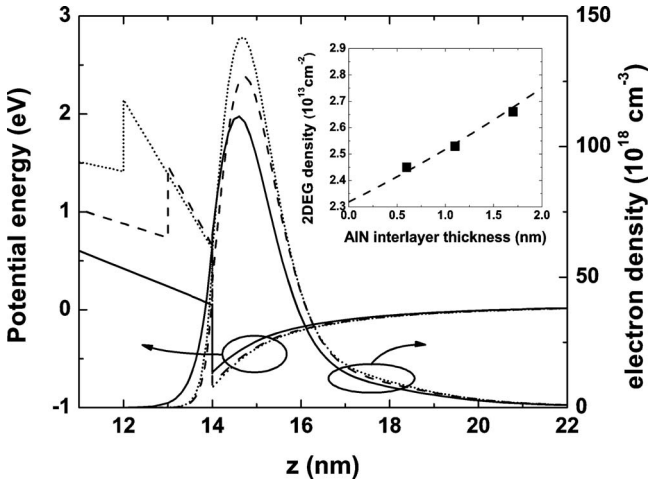

FIG. 3. Calculated band profile and 2DEG distribution along the z axis for an $Al_{0.855}In_{0.145}N/AlN/GaN$ heterostructure for 0, 1, and 2 nm AlN interlayer thicknesses. The inset shows the calculated (dashed line) and experimental (black squares) 2DEG density increase due to the increasing interlayer thickness.

increases as a function of the AlN interlayer thickness variation. Obviously, the AlN interlayer prevents the electron wave function from penetrating into the AlInN barrier due to an increased effective mass and band offset. Thus, without an interlayer, ~8.7% of the electron density distribution penetrates into the AlInN barrier, while for a 1 nm interlayer, the percentage is only ~2.5% with a penetration depth of ~0.7 nm; i.e., the electrons only penetrate into the interlayer. For interlayer thicknesses of >1 nm, the electron wave function again approaches the heterointerface due to the increased 2DEG density. This confirms, indeed, the experimentally found optimal AlN interlayer thickness of ~1 nm, where the 2DEG exhibits a mobility of ~1170 $cm^2/V\,s$ and a sheet resistance as low as 194 $\Omega/\square$ at 300 K.[4]

Figure 4 shows the 2DEG density deduced from low-frequency (0.3 kHz) electrochemical C-V measurements for 6 and 14 nm thick barriers for different compositions (black squares). The 2DEG densities range from $\sim 2.2\times10^{13}$ up to $\sim 3.5\times10^{13}$ cm^{-2} for 14 nm thick barriers, for an indium content varying between 21% and 7%, respectively. For 6

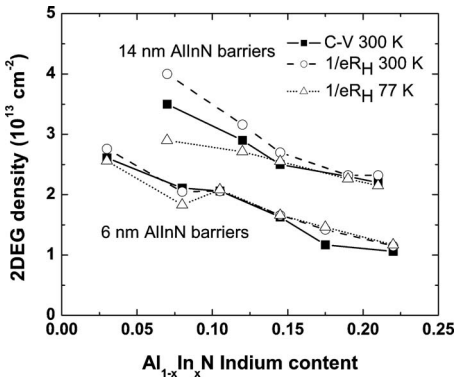

FIG. 4. 2DEG density integrated from 0.3 kHz electrochemical C-V measurements at 300 K (black squares), and Hall coefficient $1/eR_H$ measurements at 77 K (open triangles) and 300 K (open circles) for 6 and 14 nm thick AlInN barriers.

nm thick barriers, 2DEG densities between $\sim 1.1\times10^{13}$ and $\sim 2.6\times10^{13}$ cm^{-2} were found for a barrier indium composition between 22% and 3%, respectively. Note that the precision on the measured 2DEG densities is $\pm 0.1\times10^{13}$ cm^{-2} due to statistical composition and thickness fluctuations. Additionally, the Hall coefficient $1/eR_H$ was measured in the Van der Pauw geometry at 300 K (open circles) and 77 K (open triangles) for all samples. A difference rising up to 25% is found between C-V and Hall coefficient measurements (e.g., for the 14 nm thick AlInN barrier sample with 7% In). Such deviation has already been reported by other authors for AlGaN/GaN 2DEGs.[25] This can have several origins. In general, the Hall coefficient will only coincide with 2DEG densities derived from C-V if (i) the surface potential is the same, (ii) the structure is undoped, (iii) only one conducting layer with isotropic resistivity contributes to the current, and (iv) the magnetic field is sufficiently high for the scattering factor r_H to become unity. Indeed, an in-plane direction dependence of the 2DEG mobility can lead to erroneous experimental 2DEG densities.[26,27] Such an anisotropy of the mobility can occur if the interface roughness scattering is the main scattering mechanism[22] and the heterointerface possesses nonisotropic correlation lengths.[28] Indeed, in our case, atomic force microscopy measurements reveal a strong anisotropy of the correlation length of the underlying GaN buffer surface (not shown) that could be responsible for the experimental deviations. On the other hand, self-consistent Schrödinger–Poisson calculations reveal the possible occupation of the first excited state. Occupation of the first excited subband is also experimentally found in AlGaN/GaN and AlGaN/AlN/GaN heterostructures.[29,30] For 6 nm $Al_{0.855}In_{0.145}N/AlN/GaN$ heterostructures, ~9% of the electrons are in the first excited state. This amount increases to ~12% if the barriers are 14 nm thick and to ~15% for a 14 nm $Al_{0.93}In_{0.07}N/AlN/GaN$ heterostructure. An occupied excited state would, hence, result in a second conducting layer thereby decreasing $1/eR_H$ according to a simple two-layer model.[31] Furthermore, the influence of residual doping in the barrier might also play a role. By using the relation $V=eN_D/2\varepsilon\varepsilon_0\cdot x_d^2$ in the depletion approximation,[31] where x_d is the width of the depletion region and V is the total voltage across the depletion region, the minimum residual donor concentrations for those thin layers, which are clearly detectable via C-V can be estimated. If one assumes a linear regime of the $1/C^2$ plot of ~0.2 V, this would correspond to minimum residual donor densities of $\sim 1.5\times10^{18}$ cm^{-3} for 14 nm LM barriers and $\sim 7\times10^{18}$ cm^{-3} for 6 nm LM barriers. Below this threshold, donors might be present but cannot clearly be detected. Hence, electrons activated from residual donors might affect the 2DEG density.

However, even in the absence of any residual doping, an intrinsic change of the 2DEG density as a function of temperature is to be expected. This effect mainly has two origins: the first one is the temperature dependence of the lattice constants and, thus, the change of the barrier strain with temperature, which will induce a change in piezoelectric polarization.[32] Second, the strain state and the temperature will also affect the band offset and, hence, influence the confinement of carriers at the heterointerface.[33] For pseudomor-

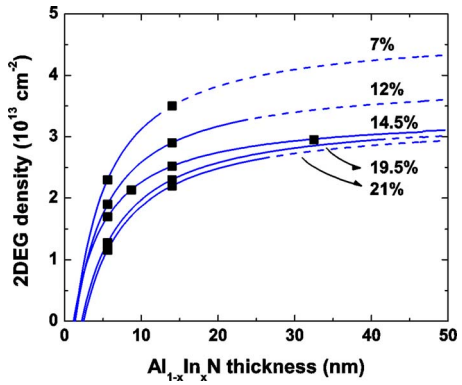

FIG. 5. (Color online) 2DEG density (deduced from *C-V* measurements) at room temperature for 6, 9, 14, and 33 nm thick $Al_{1-x}In_xN$ barriers on GaN epilayers (black squares). Blue lines correspond to a fit by using Eq. (4). A full line turning into a dashed line indicates that the critical thickness t_{cr} beyond which pseudomorphic AlInN layers are expected to relax is achieved for the respective composition.

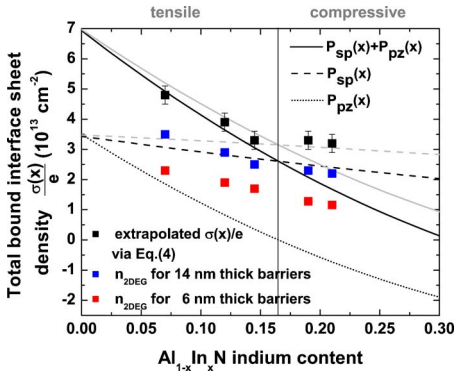

FIG. 6. (Color online) Lines correspond to spontaneous (---) and piezoelectric (···) polarization charges and the sum of both (—) at room temperature. Black lines indicate the behavior of a random alloy, while light gray lines correspond to a CuPt-like structure for the AlInN alloy. 2DEG densities for 6 nm thick (red squares), 14 nm thick (blue squares) AlInN barriers, and the extrapolated total bound sheet density $\sigma(x)/e$ (black squares) are indicated.

phic barriers, the effect of the temperature on the total bound sheet charge leads to a significantly larger influence on the 2DEG density than the temperature dependence of the band offset. By using interpolated values for the elastic and piezoelectric constants, the piezoelectric polarization charges for a LM AlInN/GaN heterostructure should increase by an amount $\Delta(\sigma/e)\sim 0.15\times 10^{13}$ cm^{-2} from 10 to 300 K and $\Delta(\sigma/e)\sim 0.11\times 10^{13}$ cm^{-2} from 77 to 300 K, respectively. If the barrier layers are unstrained and the potential at the AlInN-air interface does not change with temperature, then a decrease in the band offset with temperature would lead to a decrease in the 2DEG density of $\sim 0.005\times 10^{13}$ cm^{-2} from 77 to 300 K. For the 6 nm thick barrier layers in the compressive regime ($x=19.5\%$ and 21%), we measure, indeed, a decrease in the 2DEG density of $\sim 0.01\times 10^{13}$ cm^{-2} from 77 to 300 K, likely because the influence of the electrons activated from the residual donors is less pronounced than for the respective 14 nm thick barriers.

An aspect detrimental to the recovery of the total polarization charge density limit is the large misfit of layers, which are not grown LM to GaN. Indeed, the latter possess a critical thickness t_{cr} beyond which they tend to relax. A simple estimate is given by the relation $t_{cr}\sim b_e/2\varepsilon_{\|}$, with the Burgers vector $b_e=0.318\ 25$ nm.[34] Thus, for the growth of AlN on GaN, t_{cr} is ~6.5 nm.[22] The incorporation of indium allows, thus, increase in the barrier thickness. Especially for a vanishing $\varepsilon_{\|}$ in the LM case, very thick layers can be grown (experimentally more than 500 nm), allowing recovering a 2DEG density close to the total polarization charge density limit. Figure 5 shows fits (blue lines) of the 300 K *C-V* data (black squares) obtained by using Eq. (4) for five alloy compositions (corresponding to Table I). These fits support values for the surface potentials $e\Phi_b(x)$ with the electrolyte and for the bound interface sheet density $\sigma(x)/e$. These results are summarized in Table II. When the full line turns into a dashed line, it indicates the critical thickness t_{cr} for a given In content either in the tensile or in the compressive regime beyond which an onset of relaxation can be expected if the barrier layers are grown fully pseudomorphic to GaN. Especially in the compressive regime, we point out that the experimental 2DEG densities for 14 nm thick AlInN barriers are larger than expected from a pure pseudomorphic behavior. The critical thickness t_{cr}, derived by using the in-plane strain values deduced from Table I is also given in Table II. More sophisticated models of strain relaxation mechanisms could potentially be applied.[35] Note that $e\Phi_b$ ranges up to 3.1 eV. Such high values are also experimentally found in AlGaN/AlN/GaN heterostructures.[20]

Figure 6 shows the 2DEG densities versus indium compositions for 6 and 14 nm thick AlInN barriers and the extrapolated total bound sheet density $\sigma(x)/e$ obtained by using Eq. (4). Error bars indicate an uncertainty of $\pm 0.3\times 10^{13}$ cm^{-2} for the extrapolated $\sigma(x)/e$. Additionally, the spontaneous $P_{sp}(x)$ and the piezoelectric $P_{pz}(x)$ polarizations

TABLE II. Critical thickness t_{cr} for relaxation, 2DEG densities deduced from *C-V* measurements for 6 and 14 nm thick barriers, band offset at the AlInN/AlN interface, surface potential, and bound interface sheet density for five different compositions in the nearly LM regime between 7% and 21%.

Indium content (%)	t_{cr} of $Al_{1-x}In_xN$ (nm)	2DEG density (10^{13} cm^{-2}) 6 nm	2DEG density (10^{13} cm^{-2}) 14 nm	$\Delta E_{C,AlInN/AlN}$ (eV)	$e\Phi_b(x)$ (eV)	$\sigma(x)/e$ (10^{13} cm^{-2})
7	12.4	2.3	3.5	0.4	3.1	4.8
12	24.9	1.9	2.9	0.7	2.7	3.9
14.5	52.1	1.7	2.5	0.8	2.3	3.3
19.5	44.6	1.28	2.3	1.1	2.6	3.3
21	28.0	1.16	2.2	1.2	2.6	3.2

and their sum are shown based on the calculations of the macroscopic polarization for the AlInN alloy for two different atomic structures as given by Bernardini and Fiorentini[36] Indeed, these authors pointed out a strong nonlinear behavior for $P_{sp}(x)$ and $P_{pz}(x)$ depending on the atomic structure. Calculations were performed for a random alloy, i.e., a random distribution of group-III elements on the wurtzite cation sites, while anion sites are occupied by nitrogen leading to a P_{sp} bowing parameter $b_{random} \sim -0.065$ C/m^2 (black lines in Fig. 6). On the other hand, ordering effects in the AlInN alloy can lead to a significant change in $P_{sp}(x)$. Thus, for a CuPt-like structure, i.e., Al (or In) atomic planes alternating with Ga planes along the [0001] direction, b_{CuPt} is predicted to be ~ -0.337 C/m^2 (gray lines in Fig. 6). For the tensile strain regime, extrapolated $\sigma(x)/e$ values agree fairly well with the trend expected for pseudomorphic layers, i.e., a contribution from $P_{pz}(x)$ is present. On the other hand, the uncertainties on the extrapolation do not allow for drawing a conclusion for the atomic structure of the AlInN. In the compressive regime (samples D and E), the extrapolated $\sigma(x)/e$ values are much higher than expected for a pseudomorphic random alloy. Even the 2DEG densities for the 14 nm thick AlInN barriers exceed the polarization limit given by the black full line despite only a minor onset of relaxation of $\sim$10%. The exact mechanism responsible for this behavior is not known at the present stage. Elastic energy release through AlInN phase segregation could be invoked; ordering effects or roughness induced polarization charges[37] could also play a role.

IV. SUMMARY

In conclusion, high quality AlInN thin barriers with a 1 nm AlN interlayer in the 3%–23% indium composition range have been grown on GaN by MOVPE. The absence of Ga in the AlInN barrier is confirmed by SNMS and HRXRD. The lattice parameters are determined via HRXRD taking into account the residual strain of the GaN layer. The role of the AlN interlayer was pointed out by explaining the high mobility window at $\sim$1 nm interlayer thickness. The 2DEG densities range from $\sim 2.2 \times 10^{13}$ up to $\sim 3.5 \times 10^{13}$ cm^{-2} for 14 nm thick AlInN barriers and from $\sim 0.8 \times 10^{13}$ up to $\sim 2.0 \times 10^{13}$ cm^{-2} for 6 nm thick AlInN barriers, when varying the indium content from 21% to 7% for 14 nm thick barriers and from 23% to 3% for 6 nm thick barriers, respectively. Interestingly, the 6 nm thick LM AlInN barrier gives rise to a 2DEG density as high as 1.7×10^{13} cm^{-2}, which might reveal to be very useful for HEMT device processing. Furthermore, the total bound interface sheet density and the surface potential were extrapolated as lying between 3.2×10^{13} and 4.8×10^{13} cm^{-2} and 2.6 and 3.1 eV for an indium content ranging from 21% to 7%, respectively. A good agreement between the strain state of the AlInN layer and the 2DEG density formed at the heterointerface is found for the tensile regime, while experimentally found 2DEG densities for the compressive regime are larger than expected for a pseudomorphic random alloy despite only a minor onset of relaxation.

ACKNOWLEDGMENTS

This work was carried out under the UltraGaN European Project and was supported by the Swiss National Science Foundation (Contract No. 200021-107642/1). N.G. is indebted to the Sandoz Family Foundation for financial support. The authors would like to acknowledge M. Ilegems and thank R. Butté for a critical reading of the manuscript. V.D. acknowledges the support from the Swedish Research Council under Contract No. 2005–5054.

[1] M. Higashiwaki, T. Mimura, and T. Matsui, Jpn. J. Appl. Phys., Part 2 **45**, L1111 (2006).
[2] J. Kuzmík, IEEE Electron Device Lett. **22**, 510 (2001).
[3] F. Bernardini, V. Fiorentini, and D. Vanderbilt, Phys. Rev. B **56**, R10024 (1997).
[4] M. Gonschorek, J.-F. Carlin, E. Feltin, M. A. Py, and N. Grandjean, Appl. Phys. Lett. **89**, 062106 (2006).
[5] F. Medjdoub, D. Ducatteau, C. Gaquière, J.-F. Carlin, M. Gonschorek, E. Feltin, M. A. Py, N. Grandjean, and E. Kohn, Electron. Lett. **43**, 309 (2007).
[6] N. Sarazin, O. Jardel, E. Morvan, R. Aubry, M. Laurent, M. Magis, M. Tordjman, M. Alloui, O. Drisse, J. Di Persio, M. A. di Forte Poisson, S. L. Delage, N. Vellas, C. Gaquière, and D. Théron, Electron. Lett. **43**, 1317 (2007).
[7] J.-F. Carlin and M. Ilegems, Appl. Phys. Lett. **83**, 668 (2003).
[8] R. Butté, J.-F. Carlin, E. Feltin, M. Gonschorek, S. Nicolay, G. Christmann, D. Simeonov, A. Castiglia, J. Dorsaz, H. J. Buehlmann, S. Christopoulos, G. Baldassarri Höger von Högersthal, A. J. D. Grundy, M. Mosca, C. Pinquier, M. A. Py, F. Demangeot, J. Frandon, P. G. Lagoudakis, J. J. Baumberg, and N. Grandjean, J. Phys. D: Appl. Phys. **40**, 6328 (2007).
[9] S. Hofmann, Rep. Prog. Phys. **61**, 827 (1998).
[10] K. Lorenz, N. Franco, E. Alves, I. M. Watson, R. W. Martin, and K. P. O'Donnell, Phys. Rev. Lett. **97**, 085501 (2006).
[11] S. Pereira, M. R. Correia, E. Pereira, K. P. O'Donnell, E. Alves, A. D. Sequeira, and N. Franco, Appl. Phys. Lett. **79**, 1432 (2001).
[12] O. Brandt, P. Waltereit, and K. Ploog, J. Phys. D **35**, 577 (2002).
[13] W. Shan, R. J. Hauenstein, A. J. Fischer, J. J. Song, W. G. Perry, M. D. Bremser, R. F. Davis, and B. Goldenberg, Phys. Rev. B **54**, 13460 (1996).
[14] B. Gil and O. Briot, Phys. Rev. B **55**, 2530 (1997).
[15] V. Darakchieva, M. Beckers, M. Xie, L. Hultman, B. Monemar, J.-F. Carlin, E. Feltin, M. Gonschorek, and N. Grandjean, "Effects of strain and composition on the lattice parameters and applicability of Vegard's rule in Al-rich $Al_{1-x}In_xN$ films grown on sapphire," J. Appl. Phys. (in press).
[16] C. Gadanecz, J. Bläsing, A. Dadgar, C. Hums, and A. Krost, Appl. Phys. Lett. **90**, 221906 (2007).
[17] K. Lorenz, N. Franco, E. Alves, S. Pereira, I. M. Watson, R. W. Martin, and K. P. O'Donnell, "Relaxation of compressively strained AlInN on GaN," J. Cryst. Growth (submitted).
[18] O. Ambacher, J. Majewski, C. Miskys, A. Link, M. Hermann, M. Eickhoff, M. Stutzmann, F. Bernardini, V. Fiorentini, V. Tilak, B. Schaff, and L. F. Eastman, J. Phys.: Condens. Matter **14**, 3399 (2002).
[19] L. Shen, S. Heikman, B. Moran, R. Coffie, N.-Q. Zhang, D. Buttari, I. P. Smorchkova, S. Keller, S. P. DenBaars, and U. K. Mishra, IEEE Electron Device Lett. **22**, 457 (2001).
[20] Z. H. Wu, M. Stevens, and F. A. Ponce, Appl. Phys. Lett. **90**, 032101 (2007).
[21] W. Terashima, S.-B. Che, Y. Ishitani, and A. Yoshikawa, Jpn. J. Appl. Phys., Part 2 **45**, L539 (2006).
[22] Y. Cao and D. Jena, Appl. Phys. Lett. **90**, 182112 (2007).
[23] Y. C. Kong, Y. D. Zheng, C. H. Zhou, S. L. Gu, R. Zhang, P. Han, Y. Shi, and R. L. Jiang, Appl. Phys. A: Mater. Sci. Process. **84**, 95 (2006).
[24] NEXTNANO^3 device simulation package; see http://www.nextnano.de and http://www.wsi.tu-muenchen.de/nextnano3/.
[25] G. Franssen, J. A. Plesiewicz, L. H. Dmowski, P. Prystawko, T. Suski, W. Krupczynski, R. Jachymek, P. Perlin, and M. Leszczynski, J. Appl. Phys. **100**, 113712 (2006).
[26] Y. Sato and S. Sato, Jpn. J. Appl. Phys., Part 1 **40**, 4256 (2001).
[27] O. Bierwagen, R. Pomraenke, S. Eilers, and W. T. Masselink, Phys. Rev. B **70**, 165307 (2004).
[28] M. N. Gurusinghe, S. K. Davidsson, and T. G. Andersson, Phys. Rev. B

72, 045316 (2005).
[29]C. P. Jiang, S. L. Guo, Z. M. Huang, J. Yu, Y. S. Gui, G. Z. Zheng, J. H. Chu, Z. W. Zheng, B. Shen, and Y. D. Zheng, Appl. Phys. Lett. **79**, 374 (2001).
[30]T. W. Kim, D. C. Choo, Y. R. Jang, K. H. Yoo, M. H. Jung, Y. H. Cho, J.-H. Lee, and J.-H. Lee, Solid State Commun. **132**, 67 (2004).
[31]P. Blood and J. W. Orton, *The Electrical Characterization of Semiconductors* (Academic, London, 1992).
[32]D. Chen, B. Shen, K. Zhang, Y. Tao, X. Wu, J. Xu, R. Zhang, and Y. Zheng, Jpn. J. Appl. Phys. **45**, 18 (2006).
[33]M. J. Wang, B. Shen, F. J. Zhu, Y. Wang, J. Xu, S. Huang, Z. J. Yang, K. Xu, and G. Y. Zhang, Appl. Phys. A: Mater. Sci. Process. **88**, 715 (2007).
[34]J. Singh, *Physics of Semiconductors and Their Heterostructures* (McGraw-Hill, New York, 1992), p. 734.
[35]A. Fischer, H. Kuhne, and H. Richter, Phys. Rev. Lett. **73**, 2712 (1994).
[36]F. Bernardini and V. Fiorentini, Phys. Rev. B **64**, 085207 (2001).
[37]D. N. Quang, N. H. Tung, V. N. Tuoc, N. V. Minh, and P. N. Phong, Phys. Rev. B **72**, 115337 (2005).